SEMARAK ILMU PUBLISHING

Semarak Engineering Journal

Journal homepage:
https://semarakilmu.my/index.php/sej/index
ISSN: 3036-0145

Optimally staggered arrangement of longitudinally finned flat tubes in laminar forced convection

Ahmed Hasan Ahmed[1,*], Maki H. Zaidan[2], Manar S.M. Al-Jethelaha[2]

[1] Northern Technical University, Technical Institute, Renewable Energy Research Unit, Hawija, Iraq
[2] College of Eng., Department. of Mech. Eng., Tikrit University, Tikrit, Iraq

ARTICLE INFO

Article history:
Received 20 November 2025
Received in revised form 29 January 2026
Accepted 30 February 2026
Available online 14 May 2026

Keywords:

Constructal Design; Flat Tube; External Flow; FVM; downstream Fin Length; Laminar Forced Convection

ABSTRACT

Through Constructal Design, this work investigates the impact of the downstream fin length of longitudinally finned flat tubes in maximizing the heat transfer density and minimizing pressure drop under external laminar forced convection flow. The flow is assumed to be two-dimensional, steady, and incompressible; a constant Prandtl number defines thermophysical properties. The flow arises due to a pressure drop expressed in the Bejan number. The conservation equations are solved numerically by the finite volume method (FVM) using a commercial CFD package (ANSYS 2021/R2). The range of the longitudinal pitch-to-diameter ratio (SL/D) is considered of 4.0, ST/DT=3.0, θds=0.52, Lu/DT=0.8, and 0.4≤ Ld/DT ≤ 1. Reynolds numbers vary within the range of 200≤Re ≤ 1200 for each downstream fin length. An analysis was conducted on the temperature and velocity contours. The results indicate that the relative gain in the dimensionless overall heat transfer rate, Nusselt number, dimensionless pressure drops, Bejgan number, thermal-hydraulic performance factor, and horsepower is about 15%, 13%, 55%, 74%, 72%and 65%, respectively. Finally, it is concluded that the system with the highest fin length has the highest overall performance of the heat exchanger.

1. Introduction

Without heat exchangers, our modern commercial, industrial, and technological period would be incomplete, and the range of heat exchanger types available is equal to the variety of processes and applications they can be utilized in [1-7]. Heat exchanger fluid flow and heat transfer analysis have been the subject of numerous studies [8-14]. The rate of heat transfer is maximum when the distance between the bodies reaches a particular value. Relevant research was carried out based on this principle to determine the optimal spacing between hot bodies in a cross-flow [15-18]. In addition to the relative heat transfer gain reported in the oval arrangements compared to the circular ones, heat exchangers with finned elliptical tubes showed a relative pressure drop reduction of up to 30% [19-22]. Using a hybrid mathematical model for finned circular and elliptical tube arrangements based on

* *Corresponding author.*
E-mail address: ahmedhasan_hwj@ntu.edu.iq

https://doi.org/10.37934/sej.14.1.186200

energy conservation and heat transfer coefficients obtained experimentally by a naphthalene sublimation technique through a heat and mass transfer analogy, the temperature distribution and fin efficiency in one and two-row elliptic tube and plate-fin heat exchangers were calculated numerically [23-25]. Next, the fin efficiency results were contrasted with [25]. Fluid flow over a set of diamond-shaped fins was examined using the finite element method. The flow and conjugate heat transfer of a high-performance finned oval tube heat exchanger element were calculated for a three-dimensional laminar flow that was developing hydrodynamically and thermally [26-29]. Breuer [18] thoroughly examined the confined flow around a square-cross-sectioned cylinder placed inside a plane channel using two entirely distinct numerical techniques: the lattice-Boltzmann automata (LNA) approach and the finite-volume method (FVM). The finite-volume code was based on an incompressible Navier-Stokes solver for any non-orthogonal, body-fitted grid. Critical parameters such as the drag coefficient, recirculation length, and Strouhal numbers were investigated along with velocity profiles [30]. Although there are fewer studies on flat-tube heat exchangers than on circular-tube heat exchangers, it is anticipated that they will have lower air-side pressure drops and better air-side heat transfer coefficients. A flat-tube arrangement is used to experimentally examine $CHTC$ for ($1668 \leq Re \leq 3782$). A flat tube with intake airflow angles of 30°, 45°, and 90° is set up to investigate the thermal performance, a. There are 13.2, 38.5, and 99.8 W/m^2 heat fluxes. The results demonstrated that for all heat flux scenarios, the Nu numbers increase if Re increases [31]. The effects of two heat sources at constant temperature on the $CHTC$ of a $2-D$ channel with semi-circular cylinders at the following parameters: $100 \leq Re \leq 800$, 1 space 4, and Pr = 0.7. The results showed that when the semi-cylinder spacing grows, the separation curse raises the average Nusselt number S=1.5, Re [32]. The heat transfer and pressure drop for $2-D$ in-line HE employing ($ANNs$) is $10 \leq Re \leq 320$. Results are displayed for HTC and PD for St=2.5, 3.0, and 4.5 with Sl=3.0 and 6.0. The expected values for the dimensionless pressure and average Nusselt number show strong agreement with the corpus of previous studies [33]. A fluid flow experiment involving $H.T.$ is studied for $124 \leq Re \leq 622$. The HF supplies are 1935.8 W/m^2, 1016.3 W/m^2, and 354.9 W/m^2. The experimental results show that while the friction factor decreases as Re increases, the average Nu increases with Re, and heat flux supply [34]. It is expected that the pressure loss will be less than that of circular tubes because of the smaller wake area. It is projected that flat-tube heat exchangers will be less loud and prone to vibration than circular-tube heat exchangers for the same reason. In the studies above, no constructal design was observed for longitudinally finned flat tubes. A constructal design of longitudinally finned flat tubes in cross-flow is shown in this work. To maximize heat transfer density and minimize pressure drop under external laminar forced convection flow staggered topologies, the downstream fin length of longitudinally finned flat tubes is taken into consideration.

2. Mathematical Formulation

One possible way to enhance heat transmission on the air side is to use the physical model of the $SLFFTBHE$ that is seen in Fig. 1. This type of heat exchanger usually consists of multiple $SLFFTBHE$. Constant surface temperature, steady-state conditions, laminar flow, incompressibility, and negligible viscous dissipation are the essential presumptions. The physical representation of the current problem is shown in Figure 1. Heat transmission by forced convection between the intake airflow and the heated flat tube surface in a horizontal $x-y$ plane. The two-dimensional governing equations[35-38] are summarized as follows:

$$\frac{\partial u}{\partial x} + \frac{\partial v}{\partial y} = 0, \tag{1}$$

$$\rho\left(u\frac{\partial u}{\partial x}+v\frac{\partial u}{\partial y}\right)=-\frac{\partial p}{\partial x}+\mu\left(\frac{\partial^2 u}{\partial x^2}+\frac{\partial^2 u}{\partial y^2}\right), \quad (2)$$

$$\rho\left(u\frac{\partial v}{\partial x}+v\frac{\partial v}{\partial y}\right)=-\frac{\partial p}{\partial y}+\mu\left(\frac{\partial^2 v}{\partial x^2}+\frac{\partial^2 v}{\partial y^2}\right), \quad (3)$$

$$\left(u\frac{\partial t}{\partial x}+v\frac{\partial t}{\partial y}\right)=\alpha\left(\frac{\partial^2 t}{\partial x^2}+\frac{\partial^2 t}{\partial y^2}\right). \quad (4)$$

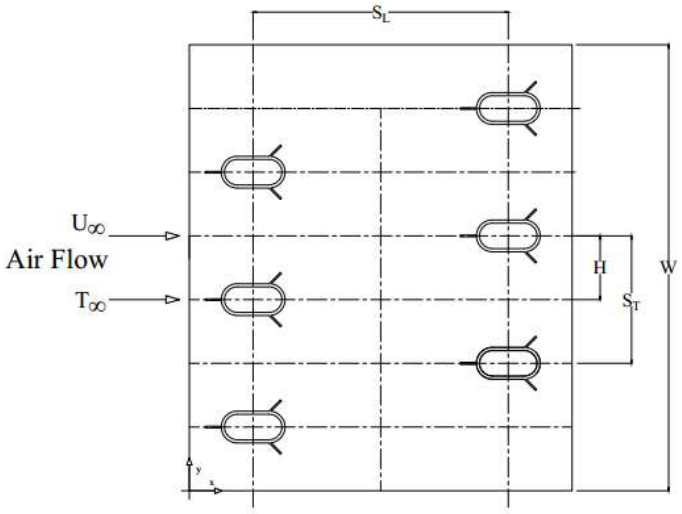

Fig. 1. Rows of $SLFFTB$ in cross-flow

To standardize Equations (1)– (4), the temperature (t) is raised by ($tw - t\infty$), the coordinates (x, y) are scaled by the finned tube diameter (dt), the velocities (u, v) are scaled by $\Delta p/\rho$, and Δp scales the pressure (p).

By utilizing the following dimensionless coordinates, velocities, pressure, and temperature, equations (1) through (4) can be non-dimensionalized:

$$X,Y=\frac{x,y}{Dt},\ U,V=\frac{u,v}{(\Delta p/\rho)^{\frac{1}{2}}},\ P=\frac{p}{p_{in}-p_{out}},\theta=\frac{t-t_o}{t_w-t_o},Be=\frac{\Delta p \mathrm{Dt}^2}{\mu\alpha},Pr=\frac{\mu Cp}{K} \quad (5)$$

Now, with the above dimensionless variables in eq. (5), Eqs. (1 –4) becomes:

$$\frac{\partial U}{\partial X}+\frac{\partial V}{\partial Y}=0 \quad (6)$$

$$U\frac{\partial U}{\partial X}+V\frac{\partial U}{\partial Y}=-\frac{\partial P}{\partial X}+\sqrt{\frac{Pr}{Be}}\left(\frac{\partial^2 U}{\partial X^2}+\frac{\partial^2 U}{\partial Y^2}\right) \quad (7)$$

$$U\frac{\partial V}{\partial X}+V\frac{\partial V}{\partial Y}=-\frac{\partial P}{\partial X}+\sqrt{\frac{Pr}{Be}}\left(\frac{\partial^2 V}{\partial X^2}+\frac{\partial^2 V}{\partial Y^2}\right) \quad (8)$$

$$U\frac{\partial \theta}{\partial X}+V\frac{\partial \theta}{\partial Y}=\frac{1}{\sqrt{(\mathrm{BePr})}}\left(\frac{\partial^2 \theta}{\partial X^2}+\frac{\partial^2 \theta}{\partial Y^2}\right) \quad (9)$$

The mean dimensionless is dominated by heat transfer and fluid flow;

$$;Re=\frac{\rho \mathrm{VD}}{\mathrm{K}\mu};\mathrm{Nu}=(h_D)/K,\ \mathrm{q_{ds}}=\frac{\mathrm{Qt}}{\mathrm{K(Ts-Tb)}} \quad (10)$$

Other dimensionless are normalized by the transverse tube diameter (DT), as the transverse pitch ratio = (ST/DT), the longitudinal pitch= (SL/DT), upstream fin length= (Lu/DT), downstream fin length (Ld/DT), dimensionless fin angle $\theta ds = \frac{\theta\pi}{180}$,

The schematic of staggered tube banks and the computational domain is shown in 'figure 1'. Boundary conditions are as follows:

$$(A): U = V = 0, \theta = 1 \quad (11)$$

$$(B): \frac{\partial U}{\partial Y} = 0, V = 0, \frac{\partial \theta}{\partial Y} = 0 \quad (12)$$

$$(I): U = 1, \frac{\partial V}{\partial X} = 0, \theta = 0 \quad (13)$$

$$(E): \frac{\partial U}{\partial X} = \frac{\partial V}{\partial X} = 0, \frac{\partial \theta}{\partial X} = 0 \quad (14)$$

Eq. (7) was solved numerically using a control volume-based finite volume method ($Fluent - CFD$) software solver. The grid is made up of triangular elements, using a $SIMPLE$ procedure.

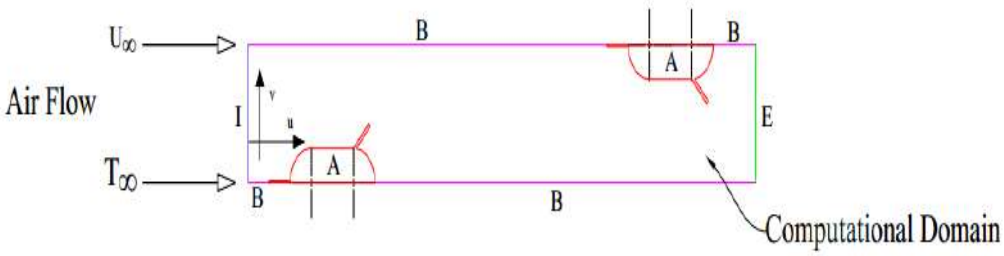

Fig. 2. Boundary Conditions for (U, V, P, and θ) around and on $LFFTBHE$ in cross-flow

3. Numerical Solution

A suitable coordinate system also forms the numerical grid that must be employed for the numerical solution of the governing equations. The Cartesian coordinate system can be utilized for simple rectangular geometries Figure 3. When the boundaries are rectangular, the use of the Cartesian coordinate system results is reasonable to specify the computational uniform of the $2D$ grid generated.

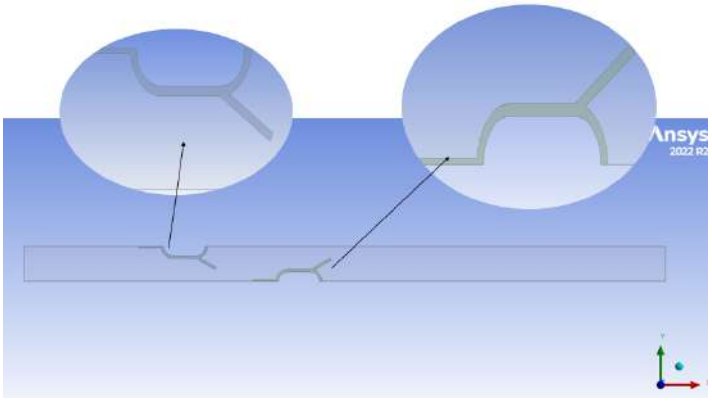

Fig. 3. Coordinate system for the $LFFTBHE$

3.1 Grid Generation

Mesh size is one of the most common problems of infinite volume analysis. There is a fine line between performing significant elements which may lead to evil. Results but fine elements show complications in the computing procedure with an extended time for the solution period. Therefore, a more precise mesh selection is Required to acquire the target results. The entire computational domain is discretized with unstructured mesh elements of more than 45000 elements Figure 4. Quadratic element order is selected for fluent. The solver has a size of $0.01mm$ for the entire computational domain and has a smooth inflation transition near tube and fin surfaces. $ANSYS\ FLUENT$ meshing offers users the option of specifying combinations of points, edge controls, surface controls, and body controls as many additional controls. Each has possibilities and can be used in various ways to influence the mesh's quality. Edge sizing controls can be given to any edge and allow for different types of Control, whereby the mesh size varies along the edge. It can use a specified element size or several divisions along the border, or a sphere of influence can control it. After the generation of the initial geometry with fluent application, the settings are $2D$, double precision, pressure-based, laminar, and use computer CPU of Intel(R) Core (TM) i7-6820HQ. The model was used in the computational domain table 1, and grid system generation is shown in Figure 4. The solver setting can be summarised in Table 2.

Table 1
The model specification of the computational domain.

Model	Settings	Model	Settings
Heat Transfer	Enabled	Time	Steady
Space	2D	Viscous	Laminar

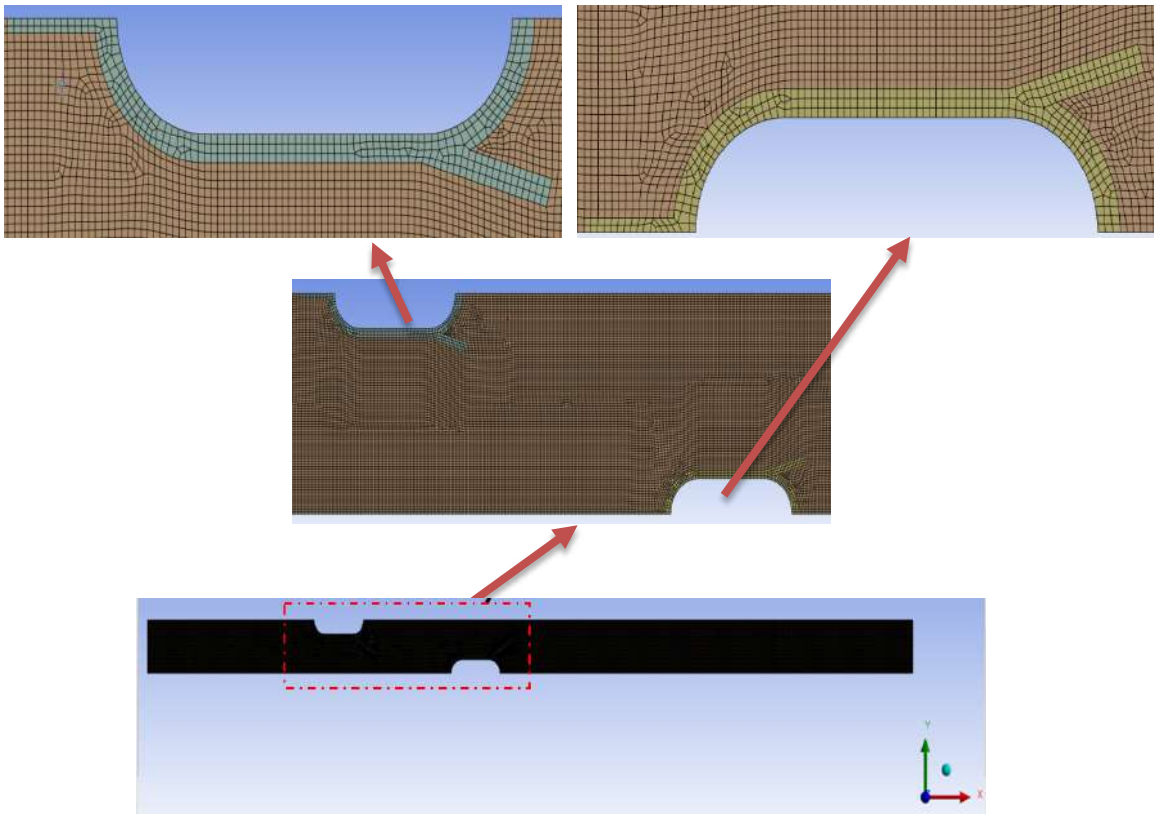

Fig. 4. Schematic of grid systems generated by finite volume method made up of triangular elements

Table 2
The solver setting for general equations.

Equations		Equations	
Density	1	Type	Coupled
Body Forces	1	Pseudo Time Method (Global Time Step)	True
Energy	0.75	Discretization Scheme	
Explicit Momentum	0.5	Pressure	Second Order
Explicit Pressure	0.5	Momentum	Second Order Upwind
Pressure-Velocity Coupling		Energy	Second Order Upwind

To ensure the stability of the solution to the governing equations, note the stability of the key to the governing equations in Table 3 and Figure 5.

Table 3
The stability setting for solving the general equations

	Value	Absolute Criteria	Convergence Status
continuity	0.0008027639	0.001	Converged
energy	1.094553e-08	1e-06	Converged
x-velocity	2.618681e-06	0.001	Converged
y-velocity	4.858248e-07	0.001	Converged

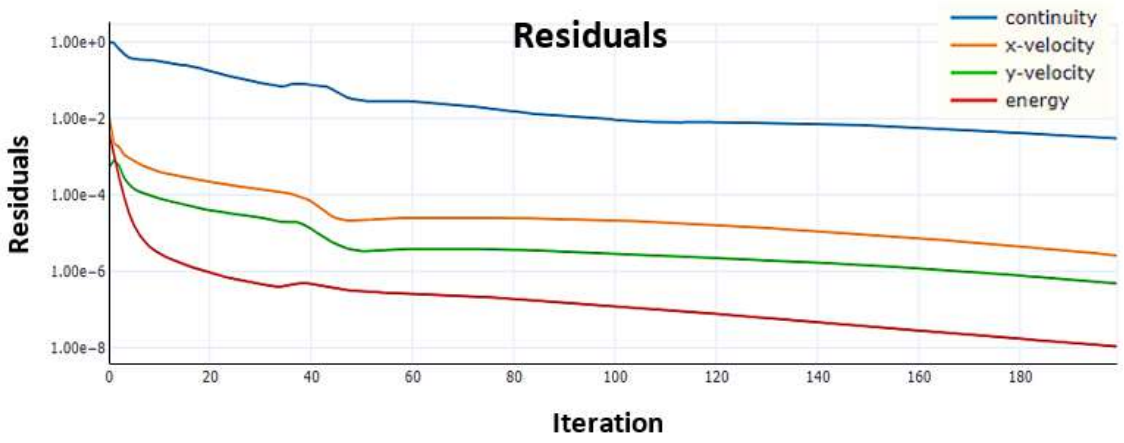

Fig. 5. The relationship between residuals and iteration for $2-D$ continuity momentum and energy equations (stability curve)

3.2 Validation Of The Computational Model

Code validation is an essential part of any numerical investigation [36,37]. The FVM formulation was presented of the computational model for heat transfer and fluid flow in $LFFTBHE$ in staggered configurations. The validation of the computational code ($ANSYS\ FLUENT\ 2022/R2$) for test problems and predictions was performed by using the developed code with exact solutions, as well as the standard issues available in previous studies. The numerical predictions established in this study were compared with those in the literature under similar tube conditions [38]. Reynolds numbers of $10 \leq Re \leq 100$ were adopted to predict the average Nusselt number. Figure 5 presents

the comparison between the present simulation results and [38]. The experimental optimization utilized under a fixed volume with geometrical parameters is shown in Table 5. The deviation increased with the increase in Reynolds's number, as shown in Figure 6. The maximum deviation values are approximately 2.62% and 2.48%. These deviations appeared because the dimensionless temperature at the inlet and outlet of heat exchanger modules was ignored, as well as the influence of the changes in thermal properties with temperature and the approximate thermal properties.

Table 4
Comparison between the present study and [38] for the geometrical parameters and average Nusselt number

				$1st$ Tube		$2nd$ Tube		$\%div.$	$\%div.$
Re	Nu	U_{max}	U	Nu_Tahsen et al. [1]	Nu_ Present CFD	Nu_tahsen	Nu_ Pres.	$2nd$	$1st$
10	0.26	0.007	0.006	5.20	5.04	3.80	3.93	3.35707	3.174603
20	0.44	0.015	0.012	5.80	5.511	5.41	5.511	1.796407	5.244057
60	1.03	0.044	0.035	10.20	10.08	8.80	8.954	1.719902	1.190476
80	1.29	0.058	0.047	11.80	11.48	10.20	10.543	3.253343	2.787456
100	1.53	0.073	0.059	12.50	12.411	11.30	11.5643	2.285482	0.717106
								2.482441	2.62274

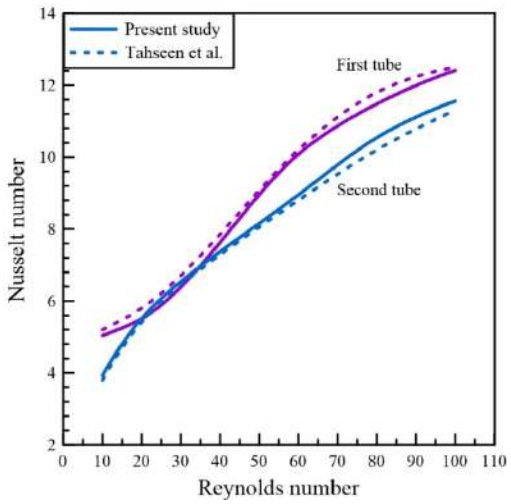

Fig. 6. Comparison between the present study with [38]for average Nusselt number with Reynolds number

3.3 Grid Independence Tests

The distribution of grid points was designed to have equal spacing (structure) in the staggered grid. General mesh testing was performed to match the grid-independent solution. The purpose is to establish an optimal mesh design within the allowable error range, achieve only a small error with minimal computation time, and obtain satisfactory results. Incorrect simulation could cause longer computation time, waste of capacity, or improper grid design. The predicted Nusselt number and balk temperature of the staggered configurations for grid systems are presented in Table 5. Increasing the grid number causes a minimal change in the Nusselt number and balk temperature. The use of these grid numbers minimizes the error and optimizes the usage of CPU resources.

Table 5
Geometric parameters of flat tube heat exchanger for model validation.

$T_{in} = 25℃, T_S = 90℃, Re = 446, \frac{St}{D_T} = 3, \frac{SL}{D_T} = 4, \frac{Lu}{D_T} = 0.6, Ld/D_T = 0.6, \hat{\theta} = 0.53, Dt = 0.01, Dh = 0.013.891,$

No	Element	Cells	Nu_1	Nu_2	T_b
1	0.0008	9,743	26.51487	21.75433	27.44252
2	0.0007	12,856	26.99066	22.26742	27.47851
3	0.0006	17,122	27.33547	22.47648	27.52426
4	0.0005	24,907	27.43764	22.58763	27.57116
5	0.0004	38,945	27.44328	22.61812	27.60632
6	0.0003	69,467	22.44362	22.61823	27.61577

4. Results and discussion

The extraction of the global ideal concerning the downstream fin length variable, the constant, and other factors took into account the optimum of the staggered finned flat tubes at a fixed volume. Table 6 and Figure 7 shows the dimensions of the fixed volume optimal technique.

Table 6
Parameters and scales of $LFFTBHE$ with down-stream fin length variable

NO.	PARAMETERS	SCALE	UNIT	NO.	PARAMETERS	SCALE	UNIT
1	ST	VARIABLE	mm	5	Ld	8	mm
2	SL	40	mm	6	θ	30^0	DEGRE
3	Lu	8	mm	7	Re	$200 \leq Re \leq 1200$	--
4	T_s	90	℃	8	T_∞	25	℃

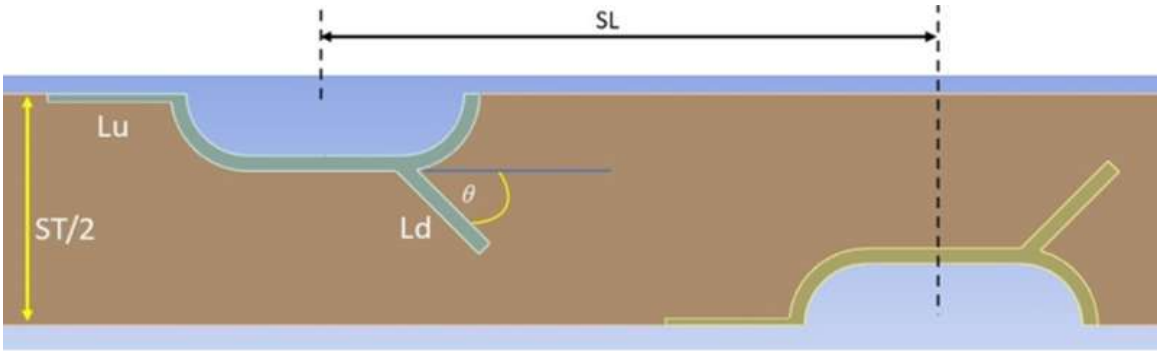

Fig. 7. Geometric of $LFFTBHE$ arrangements with down-stream fin length variable

To optimize the heat transfer density and minimize pressure drop under external laminar forced convection flow, the optimal downstream fin length of longitudinally finned flat tubes is described in this section, along with the numerical findings for temperature and velocity contours. Regarding varying downstream fin length ratio values ($0.4 \leq Ld/DT \leq 1$).

The effects of Reynolds numbers on velocity cantors and isotherms for the four modules for Ld/DT =0.4, 0.6, 0.8, and 1 are displayed in Figure 8. A broad view of floods further raises the Reynolds numbers because isotherms with lower values penetrate deeper, indicating that the cold air is closer to the hot surface. As the Reynolds number increases, the thickness of the hot layer decreases. Based on the geometry, it appears that the rear fin's length and degree of inclination have a similar effect because both lengthening the fin attempts to shift the fluid, which reduces the flow area and raises the fluid's velocity. Consequently, when this phenomenon occurs, the convection heat transfer coefficient improves; when it doesn't, the pressure drop significantly increases.

The link between the downstream fin length and the dimensionless heat transfer rate for varying Reynolds numbers is shown in Figure 9. The downstream fin length and Reynolds number have a direct relationship with the dimensionless heat transfer rate. This is because of the higher Reynolds number, which raises turbulence and raises the convection heat transfer coefficient. Turbulence increases as a result of a decrease in flow area brought on by an increase in downstream fin length. The dimensionless overall heat transfer rate reaches its maximum value, which is 285, which corresponds to the highest value of the Reynolds number and the dimensionless downstream fin length, where the amount of improvement in performance resulting from the effect of the dimensionless down-stream fin length was 15%.

The Nusselt number, which is a function of the Reynolds number in forced convection, determines the actual pipe diameter and is the primary factor governing the convection heat transfer mechanism. As a result, any increase in speed or flow area that raises the Reynolds number causes the Nusselt number to rise, which in turn raises the heat transfer rate Figure 10. Nusselt number reaches its maximum value, which is 14.3, which corresponds to the highest value of the dimensionless downstream fin length, where the amount of improvement in performance resulting from the effect of the dimensionless downstream fin length was 13%.

The link between the downstream fin length and the dimensionless pressure drop is seen in Figure 11. As per the principles of fluid mechanics, the relationship seems to be proportionate to the Reynolds number. The turbulence process may be fully understood by consulting the velocity contour and paying close attention to the transverse pitch fluid flow lines, depending on the downstream fin length. The convection heat transfer coefficient and the pressure drop are the two parameters that are the subject of all forced convection heat transfer research. However, there are three possible outcomes. The study is solely focused on heat transmission since the target is the heat transfer coefficient. If achieving the desired pressure drop is the only objective, then the analysis is pure fluid mechanics; if the effect is shared, then one of the two variables' effects cannot be disregarded. The dimensionless pressure drop reaches its maximum value, which is 14.8, corresponding to the lowest value of the Reynolds number and to the highest value of dimensionless down-stream fin length, where the amount of improvement in performance resulting from the effect of the dimensionless down-stream fin length reached 55%.

In fluid mechanics, the dimensionless pressure drop and the Began number—which indicates how much power will be used on the system—are the two key variables to learn about. Particularly on the air side of the heat exchangers, where the flow resistance is essentially nonexistent, and the heat resistance reaches 95%, the convective heat transfer coefficient is frequently the goal. At low speeds, the Began number and the pressure drop share a single factor; as speed increases, they diverge by the square of the speed. As a result, the ideal length for the rear fin must be taken into account. While it is true that a large increase in distance can enhance heat transfer, suffocation may result from the flow area's narrowing, which will cause the heat to drop. This provides adequate justification for Figure 12. The above explanation can be considered sufficient for the relationship between the Began number with respect to the dimensionless down-stream at the same range of

Reynolds numbers to reach maximum value with respect to high Reynolds number of 16×10^7 with a percentage efficiency of 74%.

The relationship between the downstream fin length and the thermal-hydraulic performance factor and horsepower is shown in Figures 13 and 14. Except for the thermal-hydraulic performance factor, the statistics above clearly show that it is exactly related to the downstream fin length. The increase in fluid velocity causes an increase in friction and, consequently, a rise in pressure drop and horsepower. The dimensionless horsepower reaches its maximum value, which is 30.5, corresponding to the lowest value of the Reynolds number and to the highest value of dimensionless down-stream fin length, where the amount of increase in performance resulting from the effect of the dimensionless down-stream fin length reached72%. Explains this occurrence. However, the combined effects of pressure drop and heat transmission are what cause the thermal-hydraulic performance factor to behave inversely. The dimensionless horsepower reaches its maximum value, which is 0.14, where the decrease in performance resulting from the effect of the dimensionless downstream fin length reached 65%.

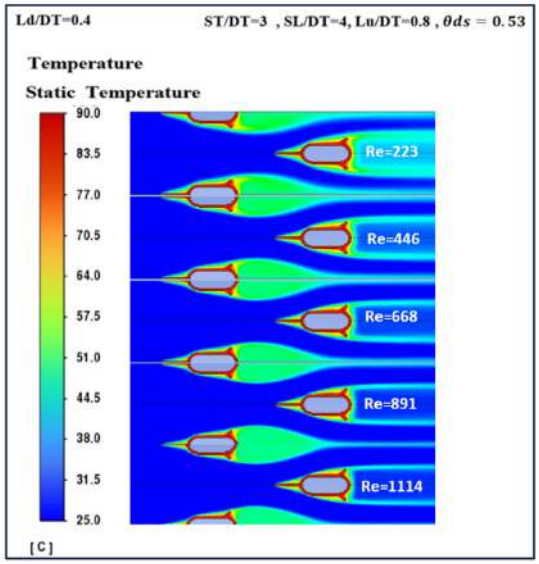

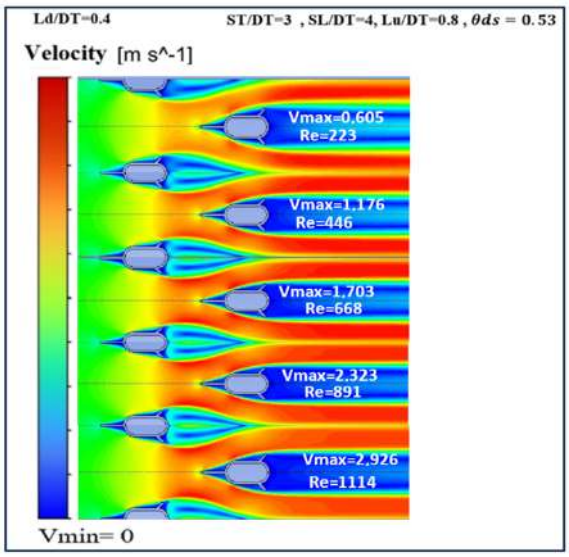

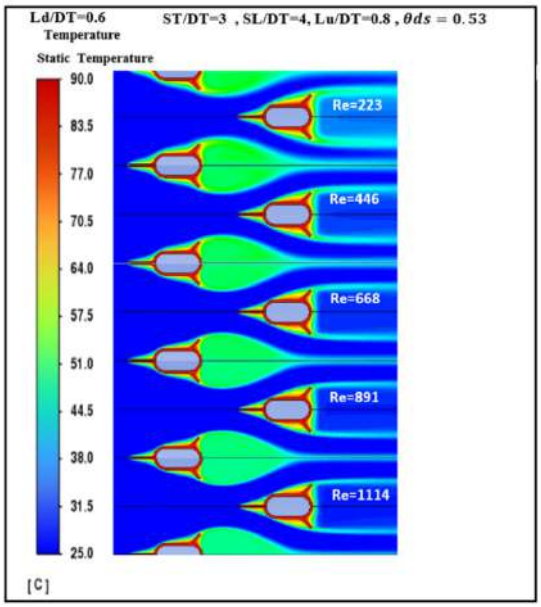

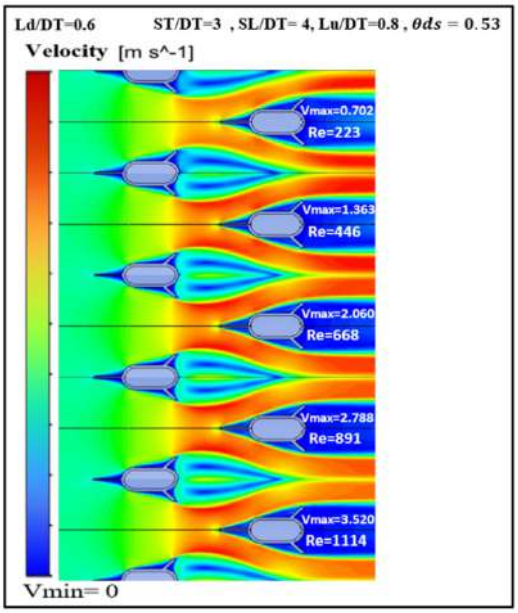

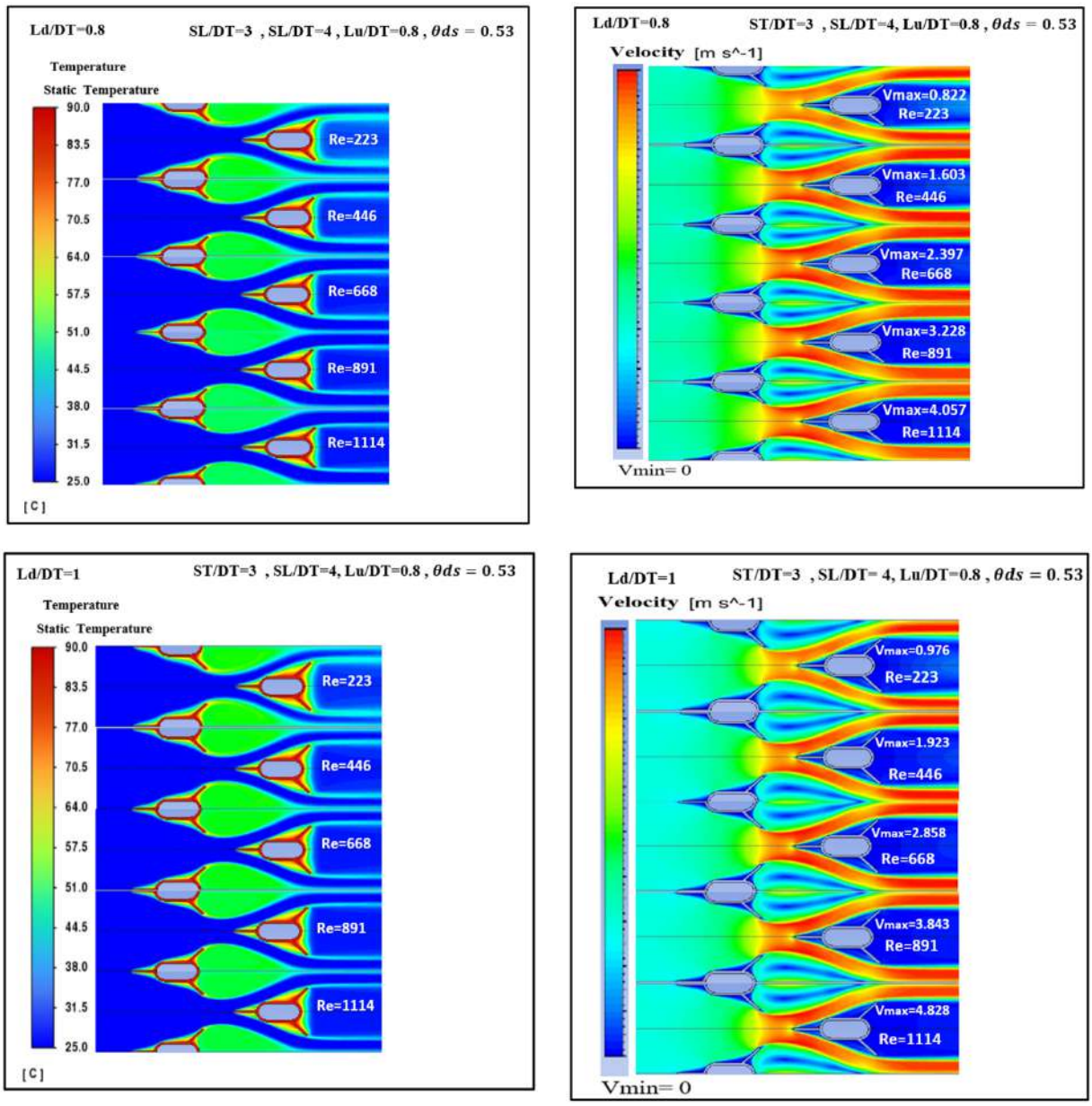

Fig. 8. Temperature and velocity contours for $0.4 \leq \frac{Ld}{DT} \leq 1$ with $\frac{SL}{DT} = 4, \frac{Lu}{DT} = 0.8,\ \frac{ST}{DT} = 3, \theta = 0.53, and\ 200 \leq Re \leq 1200$

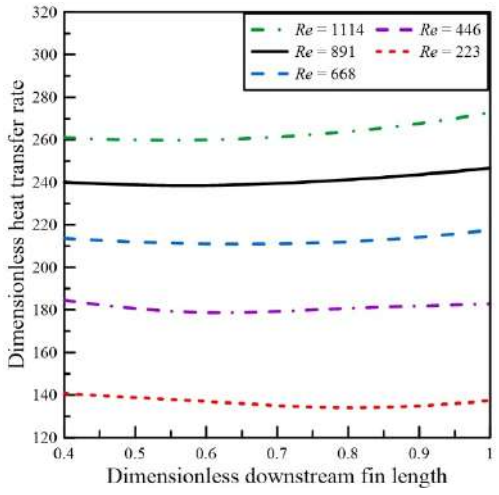

Fig. 9. Dimensionless overall heat transfer rate against dimensionless downstream fin length for various Reynolds numbers

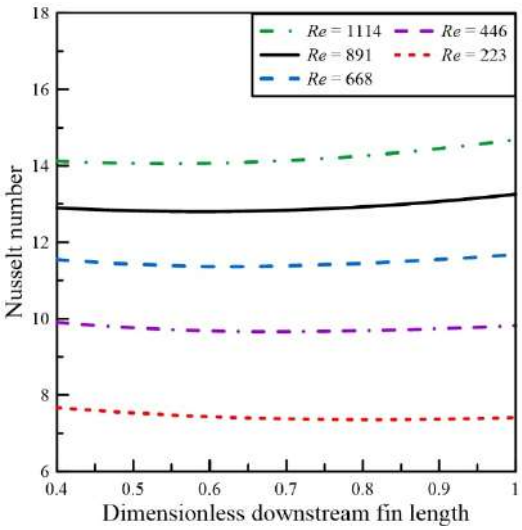

Fig. 10. Influence of Nusselt number on dimensionless downstream fin length for various Reynolds numbers

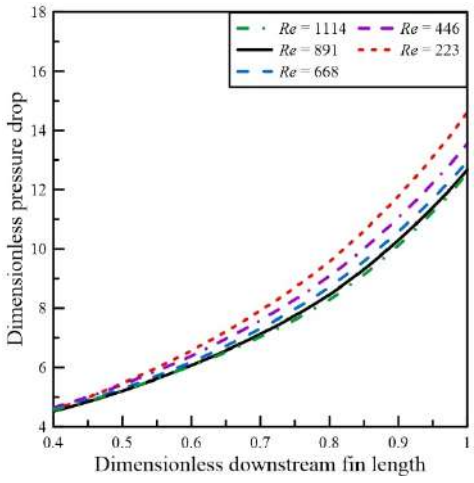

Fig. 11. Dimensionless pressure drops against dimensionless downstream fin length for various Reynolds numbers

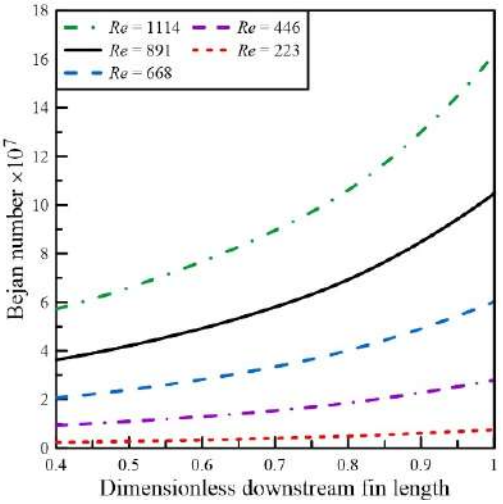

Fig. 12. Influence of Began number on dimensionless downstream fin length for various Reynolds numbers

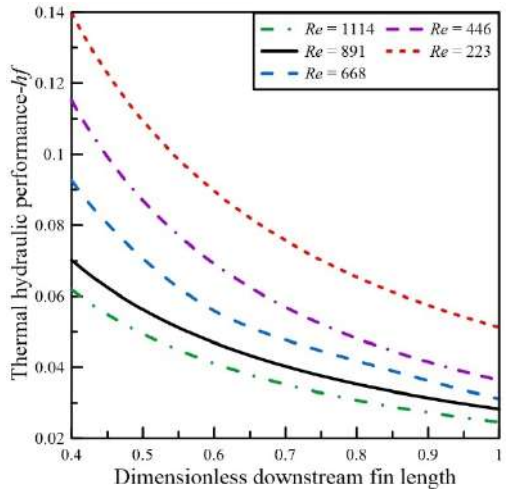

Fig. 13. Dimensionless thermal-hydraulic performance factor against dimensionless downstream fin length for various Reynolds numbers

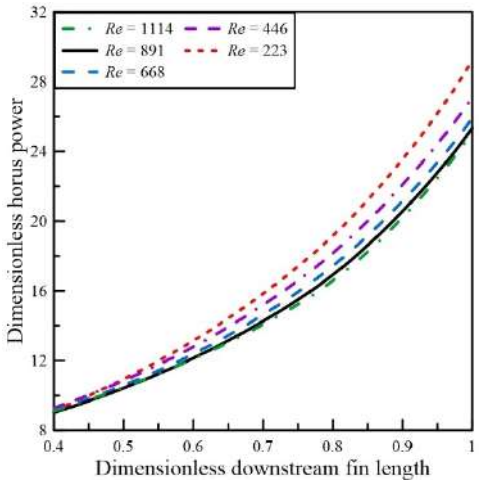

Fig. 14. Dimensionless hours power against dimensionless downstream fin length for various Reynolds numbers

5. Conclusion

A two-dimensional numerical model of the $LFFBHE$ has been successfully constructed and validated using the constructal design technique. Considering that the heat transfer density behavior for $0.4 \leq Ld/DT \leq 1$ and $200 \leq Re \leq 1200$ flow fields were demonstrated by the obtained results as a function of the change of the dimensionless downstream fin length. For the heat exchanger geometry and operating conditions considered, optimal heat transfer is attained. More heat is transported when the dimensionless Ld/DT=1. For dimensionless Ld/DT≤4, the Reynolds numbers increase, and the pressure drop decreases. For any Reynolds, the Began number rises as downstream fin length rises. The flow recirculation zone grows as downstream fin length and Reynolds numbers increase, but isothermal floods diminish as these parameters rise. As the Reynolds number rises, so does the average Nusselt number of airflows. Lastly, an increase in downstream fin length causes an increase in the average Nusselt number.

References

[1] Razera, A. L., L. A. Isoldi, L. A. O. Rocha, E. D. dos Santos, and J. V. C. Vargas. "Fluid Flow and Heat Transfer Maximization of Elliptic Cross-Section Tubes Exposed to Forced Convection: A Numerical Approach Motivated by Bejan's Theory." *International Communications in Heat and Mass Transfer* 109 (2019): 104366.

[2] Mahir, N., and Z. Altaç. "Numerical Investigation of Convective Heat Transfer in Unsteady Flow Past Two Cylinders in Tandem Arrangements." *International Journal of Heat and Fluid Flow* 29, no. 5 (2008): 1309–1318.

[3] Sahu, A. K., R. P. Chhabra, and V. Eswaran. "Effects of Reynolds and Prandtl Numbers on Heat Transfer from a Square Cylinder in the Unsteady Flow Regime." *International Journal of Heat and Mass Transfer* 52, no. 3–4 (2009): 839–850.

[4] Shah, R. K., and R. L. Webb. "Compact Heat Exchangers." In *Compact and Enhanced Heat Exchangers*. Begel House Inc. (no date given; note incomplete publication details).

[5] Bahaidarah, H. M. S., N. K. Anand, and H. C. Chen. "A Numerical Study of Fluid Flow and Heat Transfer over a Bank of Flat Tubes." *Numerical Heat Transfer, Part A: Applications* 48, no. 4 (2005): 359–385.

[6] Khan, W. A., J. R. Culham, and M. M. Yovanovich. "Fluid Flow Around and Heat Transfer from Elliptical Cylinders: Analytical Approach." *Journal of Thermophysics and Heat Transfer* 19, no. 2 (2005): 178–185.

[7] Žukauskas, A. "Heat Transfer from Tubes in Crossflow." In *Advances in Heat Transfer*, vol. 8, 93–160. Elsevier, 1972.

[8] Churchill, S. W., and M. Bernstein. "A Correlating Equation for Forced Convection from Gases and Liquids to a Circular Cylinder in Crossflow." *Journal of Heat Transfer* 99, no. 2 (1977): 300–306. (Note: journal details inferred; original citation incomplete.)
[9] Zukauskas, A., and J. Ziugzda. *Heat Transfer of a Cylinder in Crossflow*. Washington: Hemisphere, 1985.
[10] Terukazu, O., N. Hideya, and T. Yukiyasu. "Heat Transfer and Flow Around an Elliptic Cylinder." *International Journal of Heat and Mass Transfer* 27, no. 10 (1984): 1771–1779.
[11] Sharma, A., and V. Eswaran. "Heat and Fluid Flow Across a Square Cylinder in the Two-Dimensional Laminar Flow Regime." *Numerical Heat Transfer, Part A: Applications* 45, no. 3 (2004): 247–269.
[12] Rajani, B. N., A. Kandasamy, and S. Majumdar. "Numerical Simulation of Laminar Flow Past a Circular Cylinder." *Applied Mathematical Modelling* 33, no. 3 (2009): 1228–1247.
[13] Golani, R., and A. K. Dhiman. "Fluid Flow and Heat Transfer Across a Circular Cylinder in the Unsteady Flow Regime." *International Journal of Engineering Science* 3, no. 3 (2014): 8–19.
[14] Bejan, A. "The Optimal Spacing for Cylinders in Crossflow Forced Convection." *Journal of Heat Transfer* 117, no. 3 (1995): 767–770.
[15] Bejan, A., and E. Sciubba. "The Optimal Spacing of Parallel Plates Cooled by Forced Convection." *International Journal of Heat and Mass Transfer* 35, no. 12 (1992): 3259–3264.
[16] Sahel, D., H. Ameur, and W. Boudaoud. "A New Correlation for Predicting the Hydrothermal Characteristics over Flat Tube Banks." *Journal of Mechanical and Energy Engineering* 3, no. 3 (2019): 273–280.
[17] Rocha, L. A. O., F. E. M. Saboya, and J. V. C. Vargas. "A Comparative Study of Elliptical and Circular Sections in One- and Two-Row Tubes and Plate Fin Heat Exchangers." *International Journal of Heat and Fluid Flow* 18, no. 2 (1997): 247–252.
[18] Bordalo, S. N., and F. E. M. Saboya. "Pressure Drop Coefficients for Elliptic and Circular Sections in One, Two and Three-Row Arrangements of Plate Fin and Tube Heat Exchangers." *Journal of the Brazilian Society of Mechanical Sciences* 21 (1999): 600–610.
[19] Saboya, S. M., and F. E. M. Saboya. "Experiments on Elliptic Sections in One- and Two-Row Arrangements of Plate Fin and Tube Heat Exchangers." *Experimental Thermal and Fluid Science* 24, no. 1–2 (2001): 67–75.
[20] Al-damook, A., and W. M. Abed. "Numerical Optimum Investigation of Hydrothermal Characteristics over a Porous Bank of Flat Tubes Heat Exchanger." *International Communications in Heat and Mass Transfer* 154 (2024): 107447.
[21] Saboya, F. E., and E. M. Sparrow. "Experiments on a Three-Row Fin and Tube Heat Exchanger." *Journal of Heat Transfer* 98, no. 3 (1976): 471–477.
[22] Rosman, E. C., P. Carajilescov, and F. E. M. Saboya. "Performance of One- and Two-Row Tube and Plate Fin Heat Exchangers." *Proceedings of the 9th Brazilian Congress of Mechanical Engineering*, 1984 (full publication details incomplete).
[23] Ahmed, A. H., M. H. Zaidan, and M. S. M. Al-Jethelah. "Heat Transfer and Fluid Flow Characteristics in a TBHE Based on Constructal Design: An Overview." *NTU Journal of Renewable Energy* 4, no. 1 (2023): 57–96.
[24] Grannis, V. B., and E. M. Sparrow. "Numerical Simulation of Fluid Flow Through an Array of Diamond-Shaped Pin Fins." *Numerical Heat Transfer* 19, no. 4 (1991): 381–403.
[25] Chen, Y., M. Fiebig, and N. K. Mitra. "Conjugate Heat Transfer of a Finned Oval Tube Part A: Flow Patterns." *Numerical Heat Transfer, Part A: Applications* 33, no. 4 (1998): 371–385.
[26] Al-Jewaree, H. M. "An Experimentally Investigate the Fin Thermal Performance to the Different Fin Spaces by Natural Convections." *Al-Kitab Journal for Pure Sciences* 2, no. 1 (2018).
[27] Refaata, L., and A. M. Hussein. "Heat Transfer Enhancement of Alumina Nanofluid Flow in a Circular Tube." *Al-Kitab Journal for Pure Sciences* 2, no. 1 (2018).
[28] Eleiwi, M. A., T. A. Tahseen, M. A. Eleiwi, and L. B. Y. Aldabbagh. "Effect of Front Air Attack Angles on Heat Transfer Coefficient of the Cross-Flow of Four Flat Tube." *Heat Transfer* 50, no. 1 (2021): 638–654.
[29] Mustafa, A. W., A. A. M. Saied, and H. A. Sadiq. "Effect of the Presence of Semi-Circular Cylinders on Heat Transfer from Heat Sources Placed in Two Dimensional Channel." *Tikrit Journal of Engineering Sciences* 19, no. 4 (2012): 24–47.
[30] Tahseen, T. A., M. Ishak, and M. M. Rahman. "Estimation of Heat Transfer and Pressure Drop in an In-Line Flat Tubes Bundle by Radial Basis Function Network (RBFN)." In *Proceedings of the 4th International Conference on Mechanical Engineering*, Dhaka, Bangladesh, 2011 (full details incomplete).
[31] Tahseen, T. A., M. M. Rahman, and M. Ishak. "Experimental Study on Heat Transfer and Friction Factor in Laminar Forced Convection over Flat Tube in Channel Flow." *Procedia Engineering* 105 (2015): 46–55.
[32] Kwan, S. "Computer Simulation of Arcs in Gas-Blast Circuit-Breakers." PhD diss., University of Liverpool, 1996.
[33] Alnakeeb, M. A., M. A. Saad, and M. A. Hassab. "Numerical Investigation of Thermal and Hydraulic Performance of Fin and Flat Tube Heat Exchanger with Various Aspect Ratios." *Alexandria Engineering Journal* 60, no. 5 (2021): 4255–4265.

[34] Launder, B. E., and D. B. Spalding. "The Numerical Computation of Turbulent Flows." In *Numerical Prediction of Flow, Heat Transfer, Turbulence and Combustion*, 96–116. Elsevier, 1983.
[35] Ferziger, J. H., M. Perić, and R. L. Street. *Computational Methods for Fluid Dynamics*. 4th ed. Springer, 2019.
[36] Roache, P. J. *Verification and Validation in Computational Science and Engineering*. Vol. 895. Albuquerque, NM: Hermosa, 1998.
[37] Oberkampf, W. L., and C. J. Roy. *Verification and Validation in Scientific Computing*. Cambridge: Cambridge University Press, 2010.
[38] Tahseen, T. A., M. Ishak, and M. M. Rahman. "A Numerical Study of Forced Convection Heat Transfer over a Series of Flat Tubes Between Parallel Plates." *Journal of Mechanical Engineering and Sciences* 3 (2012): 271–280.